Silicon doped $LiNi_{0.5}Mn_{1.5}O_4$ as high-voltage cathode for Li-ion batteries

Doretta Capsoni[a*], Pietro Boni[a], Marcella Bini[a], Irene Quinzeni[a], Giovanna Bruni[a], Piercarlo Mustarelli[a]

[a] Department of Chemistry-Physical Chemistry Section, University of Pavia and CSGI, Viale Taramelli 16, 27100 Pavia, Italy

* Corresponding Author:
Capsoni Doretta
University of Pavia
Department of Chemistry-Physical Chemistry Section
Viale Taramelli 16
27100 Pavia (Italy)
e-mail: doretta.capsoni@unipv.it

KEYWORDS:

Li-Ion Batteries, High-Voltage Cathodes, Silicon-doped $LiNi_{0.5}Mn_{1.5}O_4$, cationic ordering in spinel

ABSTRACT

(metterei un cappello sui materiali 4V per inquadrare l'argomento) Silicon doped $LiNi_{0.5}Mn_{1.5-x}Si_xO_4$ samples ($0.00 \leq x \leq 0.35$) were prepared by different synthesis routes (solid state and ball milling). The X-ray diffraction investigation and structural and profile Rietveld refinement put into evidence the preferred segregation of lithium silicates in the solid state synthesis (direi prima qualcosa di positive). An effective spinel doping is instead obtained by the ball milling route: a solubility limit is reached for x = 0.10 and silicon ions preferentially occupy the 8a tetrahedral site of the spinel structure. SEM images show that, independently on the synthesis, silicon controls the particles morphology and grain size. These evidences (forse mettere quali, dimensione?) explain the improved electrochemical performances observed for the x = 0.05 samples with respect to the undoped ones.

1 - INTRODUCTION

The search of advance battery materials with higher energy density and lower cost becomes a priority in terms of the increasing application of lithium ion batteries on electric vehicles, hybrid electric vehicles and energy storage systems [1-3]. In this regard, cathode materials, and especially high voltage cathodes, are mainly required, because they play an important role in the electrochemical performance of lithium-ion battery and contribute approximately 40 % to the price of a complete cell [4-5].

The spinel cathode $LiMn_{1.5}Ni_{0.5}O_4$ with its high theoretical capacity of 146.7 mAh g^{-1} has drawn much attention due to its high operating voltage (~4.8 V) and the high intrinsic rate capability offered by the 3D lithium ion diffusion in the spinel lattice [6-7]. It can be stable in two different cubic structures: the Fd3m disordered one showing Mn^{4+} and Ni^{2+} randomly distributed on 16d octahedral sites and the ordered $P4_332$ one with Mn ions in 12b and Ni ions in 4a octahedral sites [8]. It is well asserted in the academic community that the electrochemical performances of this material are strongly related to the degree of Ni/Mn cation ordering. However, the assurance that the disordered phase displays better electrochemical performance, especially C rate capability, relative to the ordered phase is currently controversial [9-11].

The difficulties encountered with the dissolution of manganese and Jahn-Teller distortion in the 4 V $LiMn_2O_4$ cathode are suppressed in $LiMn_{1.5}Ni_{0.5}O_4$ as only Mn^{4+} and Ni^{2+} are present instead of Mn^{3+}. However, during its preparation some impurity phases, such as $Li_xNi_{1-x}O$ can form, so producing some amount of Mn^{3+} and/or oxygen vacancies that worsen its electrochemical performance, inducing low structural stability at high rates [12]. In particular, a rapid loss of capacity is detected during cycling: the possible reasons could be the manganese dissolution, oxygen loss and changes of particles morphology or crystallinity [9, 13].

To improve the electrochemical performances, various synthesis routes such as sol-gel method, the co-precipitation method and solid state have been tried [14-15]. Also anion or cation doping could be a satisfactory method to reduce the impurity formation and stabilize the disordered Fd3m phase. In the literature Al, Ga, Mg, Ti, Cr, Fe, Co, Cu, and Zn substitution for Mn and Ni ions in $LiMn_{1.5}Ni_{0.5}O_4$ has been used [10, 16-21].

Recently a couple of studies have been published concerning the beneficial role played by Si doping in $LiNi_{0.5}Mn_{1.5}O_4$ [22-23]. The Si ions stabilizes the disordered Fd3m structure, enhances the electrochemical stability and reduces the capacity fade, suppress the Mn^{3+} and/or oxygen vacancies amount, thus improving the cycling performances. Moreover, ~~the~~ Si as dopant is a non-toxic, eco-friendly and low-cost element.

In this work we synthesized $LiNi_{0.5}Mn_{1.5}O_4$ and $LiNi_{0.5}Mn_{1.5-x}Si_xO_4$ ($0 \leq x \leq 0.35$) samples by solid state and ball milling syntheses. Stated the favorable role played by Si doping on the high-voltage cathode material [22-23], we investigate the influence of the experimental conditions on the impurity phases formation and determine the real amount and distribution of silicon in the cationic framework. The samples were characterized by X-ray powder diffraction (XRPD) and SEM microscopy. Cyclic voltammetry and charge-discharge measurements were performed on the undoped and x=0.05 doped samples to evidence the influence of the synthesis route, the presence of impurities and Si amount ~~solubility~~ on the electrochemical performances.

2 - EXPERIMENTAL

2.1 SYNTHESES

$LiNi_{0.5}Mn_{1.5-x}Si_xO_4$ (x= 0, 0.05, 0.015, 0.25 and 0.35) spinels were prepared by solid state (SS) and ball milling solid state assisted (BM) syntheses.

For the SS samples preparation the procedure reported in the literature was used [24]. Nickel acetate tetrahydrate $Ni(CH_3COO)_2 \cdot 4H_2O$, manganese acetate tetrahydrate $Mn(C_4H_6O_4) \cdot 4H_2O$ and amorphous silica (Areosil OX 50) were ground in an agate mortar in proper amount to obtain the desired stoichiometry.

The mixture was heated at 500°C for 5h in oven, then lithium acetate dihydrate $Li(CH_3COO) \cdot 2H_2O$ was added to the mixture in 5wt% excess with respect to the stoichiometric amount.

The obtained mixture was then heated at 500°C for 5h, ground and sintered at 900°C for 10h and 700°C for 10h. The last isothermal process is recommended to avoid oxygen loss [25].

For the ball milling assisted synthesis stoichiometric amount of manganese dioxide (MnO_2), nickel oxide (NiO), amorphous silica (SiO_2) and lithium carbonate (Li_2CO_3, with a 5%wt excess) were placed in tungsten carbide jars and ground for 1h at 800 rpm with a Fritsch Pulverisette 7 planetary ball milling.

The powder was sintered at 800°C for 20 h in oven, then cooled at 1°C/min to room temperature.

Table 1 reports the samples composition and the acronyms used hereafter to identify the samples.

Table 1 - Acronyms used to name the samples

Synthesis	**Silicon content (x)**				
	0	**0.05**	**0.15**	**0.25**	**0.35**
Solid state	SS00	SS05	SS15	-	-
Ball milling	BM00	BM05	BM15	BM25	BM35

2.2. CATHODES AND CELL PREPARATION

The electrochemical measurements were performed on the samples showing the highest purity, as determined by XRPD, in particular BM00, SS00, BM05 and SS05. The samples were carbon-coated by using the procedure already described [26]. Briefly, sucrose (1% of the sample weight) and the active material were added to water and ethanol (1:4 volume), stirred at 75°C until complete evaporation of the solvent then treated at 350 °C for 1 h in air to obtain the desired coating.

To prepare the cathode slurry, a mixture of 70%wt of active material, 20%wt of carbon black and 10%wt of PVdF was stirred in N-metil-2-pirrolidone (NMP) for about three hours, then casted on aluminum foils and dried under vacuum at 120 °C for four hours. The cells were assembled in an Argon filled dry box (M. Braun, <1ppm O_2, <1ppm H_2O), by using 1M $LiPF_6$ dissolved in ethylene carbonate and dimethyl carbonate solution (EC:DMC = 1:1 v/v) as electrolyte and lithium foil with the same diameter of the cathode as counter-electrode.

2.3 CHARACTERIZATION METHODS

The samples were characterized by means of X-Ray powder diffraction (XRPD) by using a Bruker D5005 diffractometer with the Cu Kα radiation (40 KV, 40 mA) and a scintillation detector. The patterns were collected in the 15°-122° 2θ range with step size 0.02° and 3s/step of counting time. The Rietveld structural refinement was performed on the diffraction data by using the disordered spinel model (S.G. Fd3m) to determine the main structural parameters. The occupancies were also varied by using proper constraint to determine the silicon amount and its location on tetrahedral or octahedral sites of the spinel structure. Also the impurity weight percentages were determined, when detected.

SEM micrographs were collected on a Zeiss EVO MAH10 scanning electron microscope on Au sputtered samples.

The electrochemical properties were investigated at ambient temperature by means of cyclic voltammetry (CV) and galvanostatic charge discharge cycles using Swagelok cell.

The CV was performed with an Autolab PGSTAT30 potentiostat and the data were processed with GPES V4.9 software. The cells were cycled in 3.3-5V potential range. Galvanostatic charge/discharge cycles were obtained with an Arbin BT-2000 in a 5-3.3V potential range at different current rates.

3 - RESULTS AND DISCUSSION

3.1. STRUCTURAL CHARACTERIZATION

The XRPD patterns of the undoped and Si doped samples obtained by solid state synthesis are shown in Fig. 1.

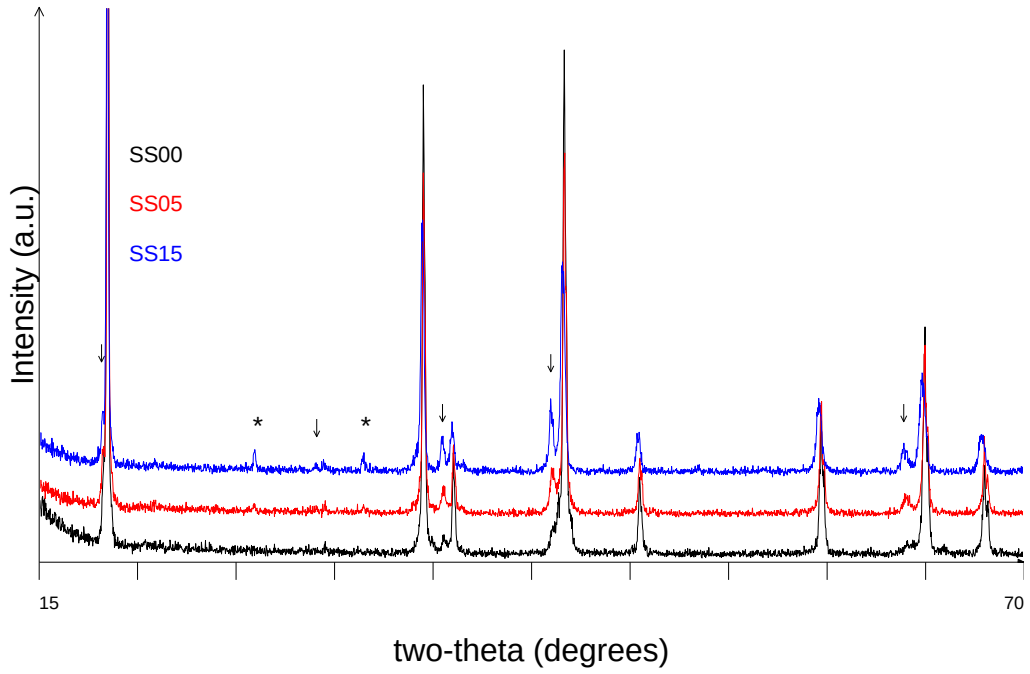

Figure 1 – XRPD patterns of undoped and Silicon doped solid state samples. Impurity phases: Ni_6MnO_8 and/or lithiated NiO (arrows), Li_2SiO_3 (*).

All the samples are crystalline, anyway the degree of crystallinity and crystallite size slowly decreases as Si content increases, as suggested by the peak broadening increase. The disordered Fd3m spinel structure (JCPDS card N. 80-2162) was obtained in all the samples, and no peaks ascribable to the $P4_332$ ordered structure (JCPDS card N. 80-2184) were detected in the 20-30° 2θ range. Some peaks due to impurity phases, mainly lithiated NiO ($Li_xNi_{1-x}O$) and Ni_6MnO_8 that show many common peaks [7], can be observed, but also silicon containing phases are detected in SS05 and SS15 samples. This evidence suggests that the silicon content expected by the synthesis is not reached in the spinel structure. The wt% amount of the crystalline phases observed in the samples can be evaluated by applying the structural and profile Rietveld refinement to the diffraction data. The obtained results are summarized in Table 2.

Table 2 – Lattice parameter, crystallite size, silicon amount n, and phase abundance obtained by Rietveld refinement on the solid state samples. The discrepancy factors are also shown.

SAMPLE	SS00	SS05	SS15
$LiNi_{0.5}Mn_{1.5-x}Si_xO_4$ (wt%)	90.0 (1)	88.6(4)	79.2(4)
n (Si)	-	0.00	0.02
a (Å)	8.1688(2)	8.1711(2)	8.1712(2)

Crystallite size (nm)	110	104	87
Lithiated NiO (wt%)	4.5(1)	5.3(3)	3.2(2)
Ni_6MnO_8 (wt%)	5.5(1)	3.9(2)	10.8(4)
Li_2SiO_3 (wt%)	-	2.3(2)	6.8(6)
R_{wp}	21.72	22.97	24.9
S	1.19	1.12	1.21

The spinel percentage obtained by the solid state synthesis is about 90% for SS00 and SS05 samples, and decreases by increasing the Si content. Anyway the total weight percentage of impurity silicon-free phases is approximately constant (about 10%). This suggests that silicon does not influence the reagents reactivity in the solid state route. The wt% amount of the Silicon containing impurity phases can be used to calculate n, the effective Si content in the spinel structure. As reported in Table 2, the n values are negligible, and the solid state synthesis fails the Si insertion in the spinel structure. This result also explains the constant value of the lattice parameter in the SS samples. Interestingly, the silicon, segregated in the Li_2SiO_3 phase, plays a role on controlling the crystal growth: smaller crystallites are obtained in the SS15 sample. The discrepancy factors R_{wp} and S reported in Table 2 prove the good agreement of the experimental and the calculated patterns. Due to the presence of significant amounts of impurity phases and the difficulty in inserting Si in the spinel structure, samples with silicon content higher than 0.15 were not prepared by SS.

The XRPD patterns of the undoped and Si doped samples obtained by ball milling synthesis are shown in Fig. 2. The disordered Fd3m spinel form, desirable to improve the electrochemical performances, is obtained. The diffraction peaks are broader than those observed in the SS samples, suggesting, as expected, lower particle sizes by ball milling procedures. This synthesis route gives purer samples than the SS one. The BM00 sample is nearly pure: only a small and broad peak at about 30°/2θ (see # in Figure 2) is observed. The phase responsible for this diffraction effect is not easily identified, and it is probably due to some Ni, Li and/or Mn mixed oxides. It should be noted that this impurity peak is not detected in the Si doped samples. An high purity is also reached for the BM05 and BM15 samples. ~~On the other hand, rather pure samples has been reported in literature by ball milling synthesis route for other dopants [9, Liu 2009, Wook 2012].~~ For higher Si content ($x > 0.15$) not negligible amount of impurity phases form, mainly lithium silicates.

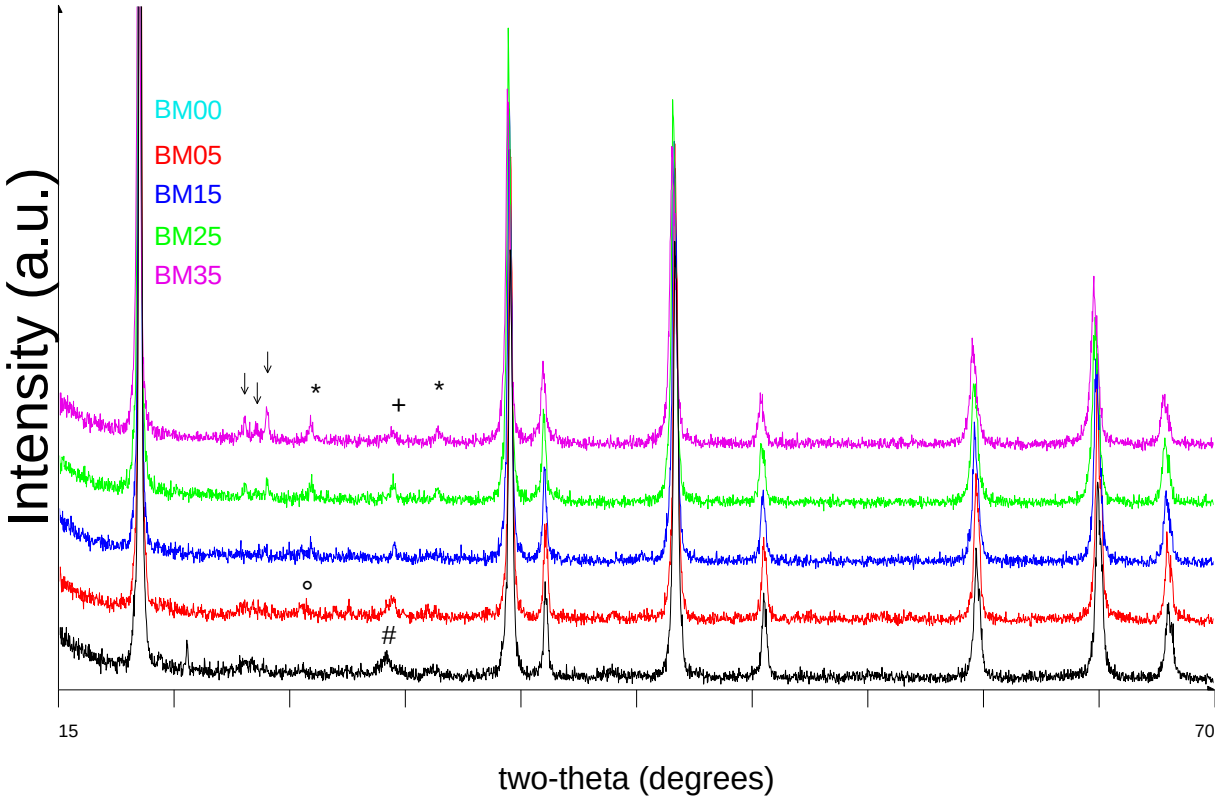

Figure 2 – XRPD patterns of undoped and silicon doped ball milled samples. Impurity phases: mixed Ni-Li-Mn oxides (#), quartz (°), Li_2SiO_3 (*), $Li_2Si_2O_5$ (arrow) and 2 2 0 reflection of the $LiNi_{0.5}Mn_{1.5-x}Si_xO_4$ phase (+).

The Rietveld refinement was applied to the diffraction data of the BM samples. The wt% amount of the impurity phases and the values of the main spinel structural refined parameters are reported in Table 3.

Table 3 – Lattice parameter, crystallite size, silicon amount, 8a site occupation and phase percentages obtained by Rietveld refinement on the ball milling samples. The discrepancy factors are also shown.

SAMPLE	BM00	BM05	BM15	BM25	BM35
$LiNi_{0.5}Mn_{1.5-x}Si_xO_4$ (wt%)	100.0	99.5(2)	97.2(2)	92.4(4)	87.3(7)
n (Si)	-	0.035	0.110	0.091	0.095
a (Å)	8.1729(2)	8.1752(2)	8.1809(2)	8.1871(2)	8.1924(4)
Si on 8a site	-	0.035(2)	0.110(2)	0.091(1)	0.095(1)
Crystallite size (nm)	77	73	72	66	54
SiO_2 (wt%)	-	0.5(2)	-	-	-

Li_2SiO_5 (wt%)	-	-	-	3.1(3)	6.7(4)
Li_2SiO_3 (wt%)	-	-	2.3(2)	4.5(4)	5.9(7)
R_{wp}	22.79	22.32	22.42	21.40	22.43
S	1.21	1.17	1.15	1.11	1.13

As concerns the quantitative evaluation of the phases present in the samples, the results in Table 3 show that the typical impurities based on Nichel Oxide (NiO and Ni1-xLixO) and Ni_6MnO_8, obtained by SS synthesis, are not observed. So the formation of undesired Mn^{3+} is avoided. In fact, Mn^{3+} gives rise to a disproportion reaction to Mn^{2+}, that is soluble in $LiPF_6$ based electrolytes and leads to electrode degradation and unwanted deposition on the negative electrode. The detection of silicon-containing impurity phases (see Table 3) also suggests that not all the Si used in the synthesis enters the spinel structure. As for the case of the SS samples, the effective amount n of Silicon present in $LiNi_{0.5}Mn_{1.5-n}Si_nO_4$ can be evaluated, known the Si amount provided in the synthesis and the percentages of silicon containing impurity phases. The n values for the BM samples are reported in Table 3. A fair agreement of x and n values for $x \leq 0.15$ is observed. For $x > 0.15$, n remains constant, due to the relevant amount of segregated lithium silicates (Table 3). This evidence suggests that silicon reaches a solubility limit in the spinel structure that could be fixed at about x = 0.10. This could explain the best electrochemical performances obtained for low silicon doping [22-23].

A careful investigation of the diffraction patterns of the doped samples puts into evidence that the diffraction peak at about 31°/2θ (220 reflection, indicated by + in Figure 2) slightly increases its intensity in the silicon doped samples, with respect to the undoped one. This peak is typically weak in the diffraction patterns of the lithium-based spinel structures as $LiNi_{0.5}Mn_{1.5}O_4$ compound, but its intensity significantly increases as the electron density on the tetrahedral site, typically occupied by Lithium, increases. These evidences suggest the possible insertion of the Silicon ions on the tetrahedral site, and not on the octahedral one, as reported in literature [23]. To further verify this hypothesis the location of the silicon ions in the spinel structure was investigated. Proper constraints to the Rietveld refinement were applied to let Silicon distribute on both the cationic sites (8a and 16d). The best refinements are obtained when Si preferentially occupies the tetrahedral 8a site. On the other hand this result is consistent with the preferred tetrahedral coordination of Si in several silicates. Moreover, the Si on the tetrahedral site of the spinel structure is responsible for an increase of disorder in the cationic framework of the spinel structure: some amount of Li should be present on the 16d sites or vacancies should remain on the 8a sites. Non capisco, vedere con Marcella. This could be fine for improving the elettrochemical stability of the high-voltage cathode. The refined lattice parameters increase as Si amount increases, in agreement with literature data concerning silicon

doping of $LiNi_{0.5}Mn_{1.5}O_4$ and $LiMn_2O_4$ spinels [22-23, 27-28]. The crystallite size determined by the Rietveld refinement demonstrates that lower particle size is obtained by the ball milling procedure with respect to the solid state one, and that silicon doping/lithium silicate impurity phases control the crystallite size. The discrepancy factors R_{wp} and S reported in Table 3 suggest the satisfactory agreement between the experimental and calculated patterns.

3.2 MORPHOLOGICAL ANALYSIS

SEM images of undoped and silicon doped x = 0.05 samples are reported in Figure 3: aggregates of particles are observed. The undoped samples show larger octahedral-shaped grains, of higher size for the SS sample, as expected. In agreement with the XRPD results, the Si doping control the particle size [23]: the grains are smaller and lose their octahedral shape. The influence of Silicon doping in controlling and homogenizing the particles morphology in $LiMn_2O_4$ compound is known [27]. Interestingly, the shape, morphology and size control of the particles is obtained by both the synthesis routes, independently on how the Si acts. In the SS procedure a composite is obtained, due to the lithium silicate segregation, while both lithium silicate segregation and substitution in the spinel structure is obtained by BM route. In the light of the XRPD and SEM results, the silicon plays a favorable role in controlling the grains morphology, either the Silicon successfully enters the spinel structure (BM sample) or segregate as a separate phase, possibly forming a spinel/lithium silicate composite.

As reported in literature [16], the formation of smaller grain sizes favored by the silicon addition could help the lithium diffusion in the cathode so improving the electrochemical performances.

The carbon coating, necessary for the electrochemical measurements, does not produce any morphological change of particle form and sizes.

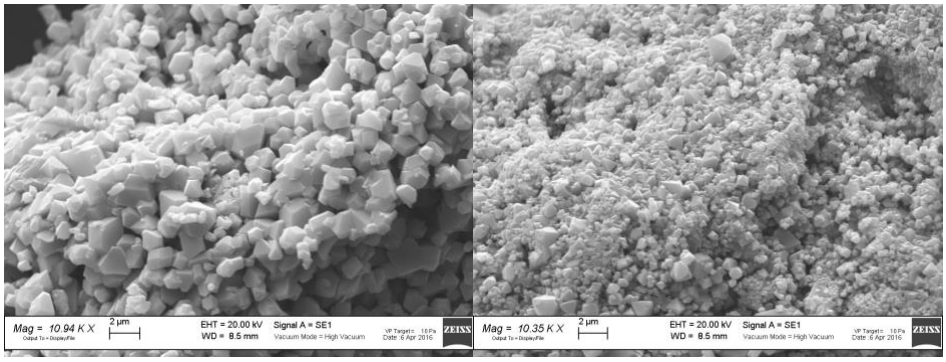

SS00 SS05

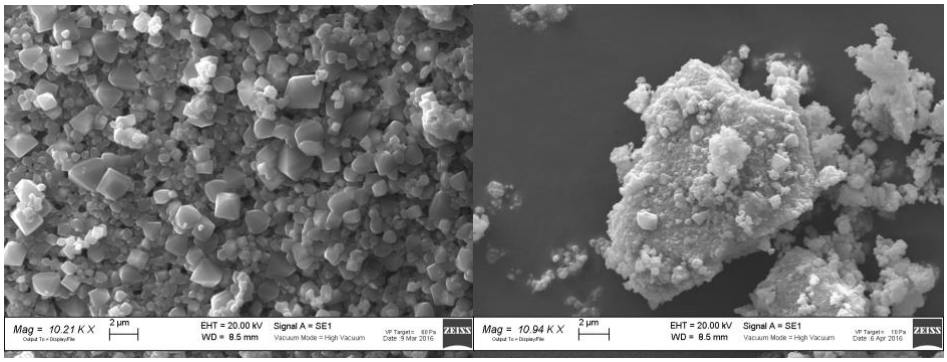

BM00 BM05

Figure 3 - SEM images of SS00, SS05, BM00 and BM05 samples

3.3 ELECTROCHEMICAL CHARACTERIZATION

The cyclic voltammetries of the x = 0.00 and 0.05 SS and BM samples (the samples showing the highest purity from both syntheses) are reported in Figure 4. The voltages of the three redox processes are reported in Table 4. As exhaustively explained in the literature [26] the peaks at about 4V correspond to Mn^{3+}/Mn^{4+} redox couple and those in the 4.7-4.8V range to the reversible oxidation/reduction of Ni^{2+}/Ni^{3+} and Ni^{3+}/Ni^{4+} redox couples.

The presence of the peak at about 4V in the SS00 and SS05 samples is due to the segregation of Ni as NiO and/or lithiated NiO, as detected by XRPD (Table 2), that causes the formation of some amount of Mn^{3+} responsible of the redox peak [29-30]. These impurity phases are not formed by BM (Table 3) and the peak at 4V is negligible. In the 4.7-4.8V range, independently on the synyhesis route, the x = 0.05 samples show sharper peaks giving better resolution of the two components than the undoped ones, and a lower potential difference between anodic and cathodic current peak maxima, suggesting faster lithium insertion/extraction kinetics. By comparing the CV curves of the x = 0.05 samples, the best performances are observed for the ball milled sample, when silicon inserts into the spinel structure, and not simply controls the particles morphology.

~~Mereover, the SS CV curves show an anodic peaks broadening higher than that observed for BM analogous. A possible explanation of this effect is reported in the literature [Wook 2012]: the lower separation of the peaks at about 4.7V may be related to an high degree of cation ordering in the spinel structure. So, from CV profiles it seems that the SS00 sample should be more ordered and with an high degree of polarization than SS05 one. This last evidence also confirms its cation ordering [wook 2012]. Controllare, non mi torna… It could be expected that when silicon is substituted in the spinel structure the disorder increases, and this is verified for the BM samples. Their lower peak broadening suggests that an higher disorder is present with respect to their SS analogous. Also in this case the~~

~~silicon insertion favors the increase of cationic disorder level, even if in a lower degree with respect to SS??? samples. In this case the polarization of BM00 and BM05 is similar~~ [13]

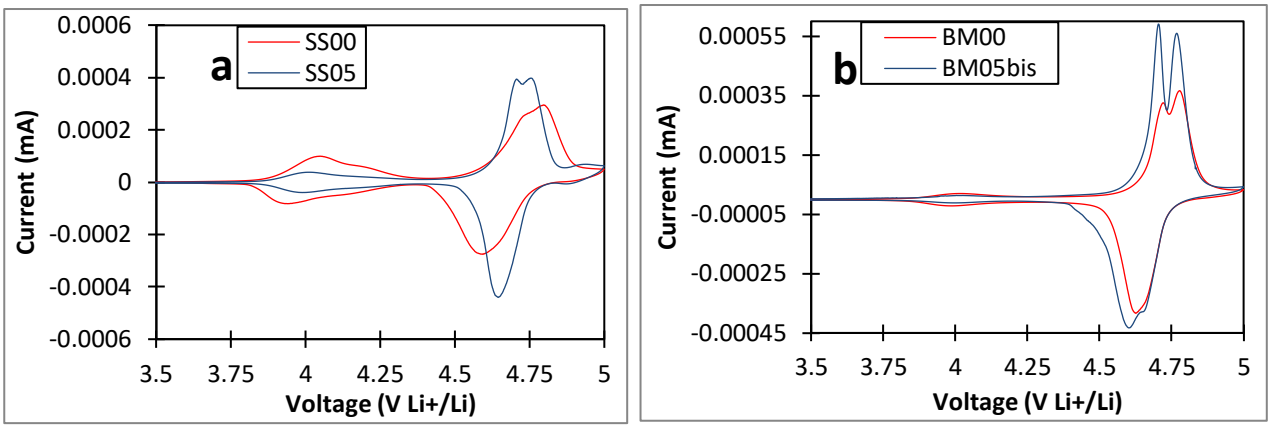

Figure 4 - Cyclic Voltammetry (second cycle) of $LiMn_{1.5}Ni_{0.5}O_4$ and $LiNi_{0.5}Mn_{1.45}Si_{0.05}O_4$ obtained by a) solid state and b) ball milling synthesis.

Table 4 - Peak voltages of the three redox processes obtained from CV curves

Peak voltage (V) Sample	Mn^{3+}/Mn^{4+} anodic	$Ni^{2+}/Ni^{3+}/Ni^{3+}/Ni^{4+}$ anodic	Mn^{3+}/Mn^{4+} cathodic	$Ni^{2+}/Ni^{3+}/Ni^{3+}/Ni^{4+}$ cathodic
SS00	4.023V	4.719V; 4.783V	3.945 V	4.605V
SS05	3.993V	4.699V; 4.74V	3.998V	4.655V
BM00	-	4.715V; 4.773V	-	4.634V
BM05	-	4.702V; 4.765V	-	4.602V; 4.66V

In Figure 5 the typical charge galvanostatic profiles are reported (utili anche quelli di scarica, ma mi sa che la strumentazione aveva problemi, non li abbiamo tutti. Devo verificare con Irene, altrimenti la togliamo). The SS sample shows a first long plateau at about 4V due to the Mn^{3+}/Mn^{4+} redox couple, then two plateaus in the range 4.68-4.75 due to the two steps nickel oxidation. For the two BM samples the galvanostatic profiles are similar: the plateau at 4V is very short, due to the low amount on Mn^{3+} present in these samples. Also in this case the plateaus due to nickel oxidation are present. The lower plateaus of SS sample suggest a faster kinetic of the involved reactions. The highest capacity is reached by the BM05 sample (138 mAh/g), but the values shown by BM00 and SS05 samples (about 130 mAh/g) are not so far.

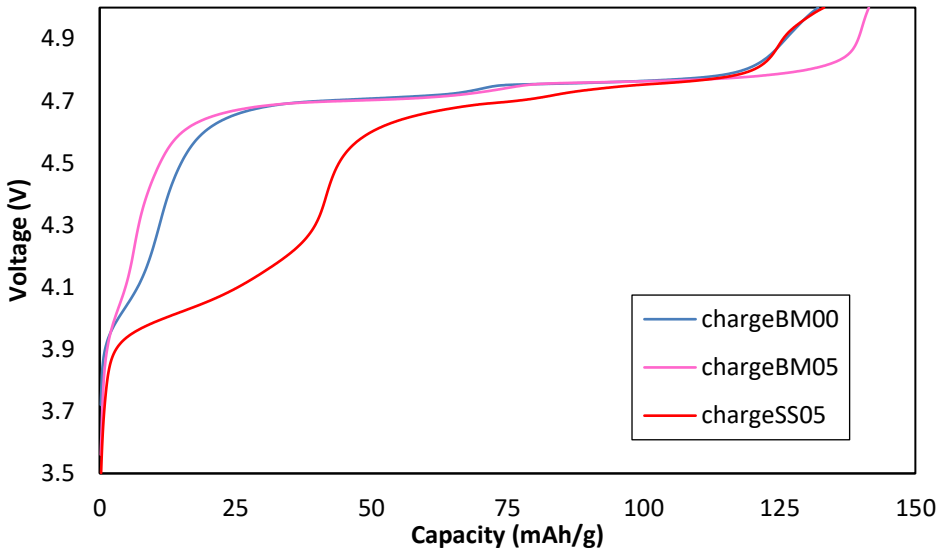

Figure 5 – Galvanostatic charge profiles of SS05, BM00 and BM05 samples (manca SS00)

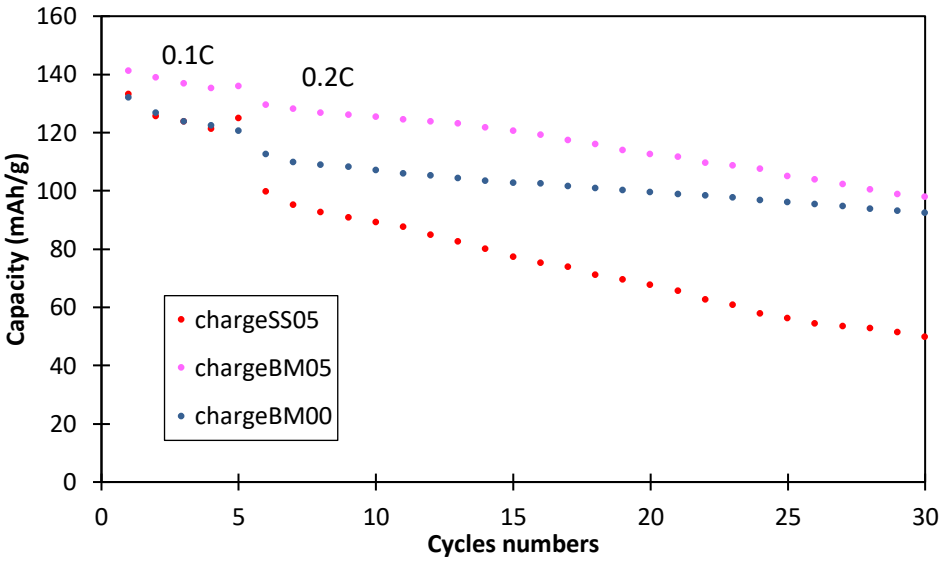

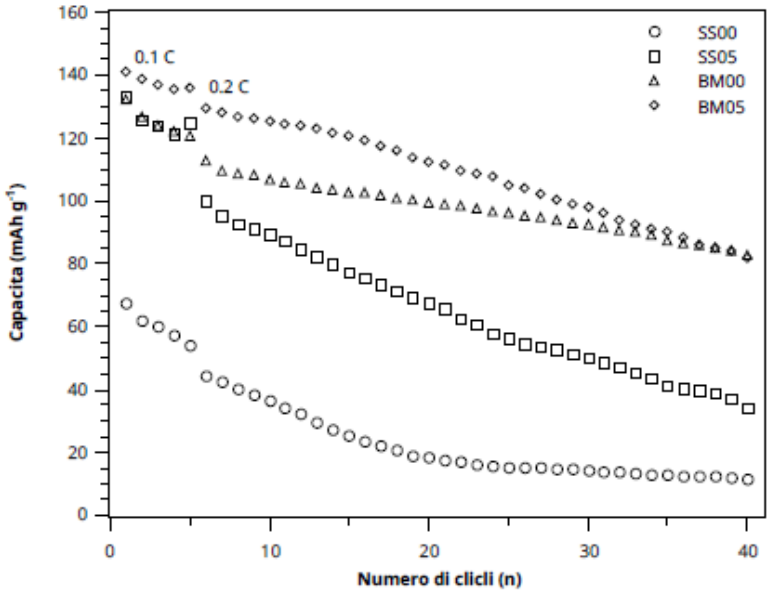

Figure 6 - Specific charge capacities of SS05, BM05, BM00 samples at 0.1C and 0.2C (manca SS00)

Figure 6 shows the charge capacity of the ball milled and doped solid state samples. In the first few cycles at 0.1 C the capacities are similar for all the samples, but slightly better for the BM05 one. The capacities approach the theoretical value of 146.7 $mAhg^{-1}$ [30]. When the C rate is increased to 0.2C the capacities fade but for the BM samples after 30 cycles a satisfactory constant value of about 110 mAh/g is maintained. A capacity retention of % is determined for BM05 and BM00 respectively. The SS samples display worse electrochemical performances with respect to the BM ones, anyway an improvement is obtained by silicon addition from the solid state synthesis, too. For the SS05 a capacity retention of % is found after 30 cycles. The electrochemical results put into evidence the double role played by silicon on the performances of the high-voltage $LiNi_{0.5}Mn_{1.5}O_4$ cathode. The best results are obtained when Si inserts in the cationic framework of the spinel structure. In this case it not only stabilizes the Fd3m crystal structure during charge/discharge processes thanks to its stronger Si-O bonds with respect to the Mn-O ones [23], but also increase the cationic disorder by occupying the tetrahedral 8a site, usually occupied by Lithium in the $LiNi_{0.5}Mn_{1.5}O_4$ compound. The solubility limit reached for n values of about 0.10 explains also the better electrochemical performances reported in literature for the composition x in the 0.05-0.15 range [22-23]. On the other hand, also when Silicon does not insert in the spinel structure and segregates as lithium silicates (SS synthesis), an improvement of the electrochemical performances is observed, possibly due to composite formation and to the size and shape control of the sample particles. The morphological control to optimize the electrochemical performance has been put into evidence in literature [23].

CONCLUSIONS

The accurate investigation and quantitative determination of the impurity phases, combined to the structural-microstructural characterization of silicon doped $LiNi_{0.5}Mn_{1.5}O_4$ compounds gives more insight into the improved electrochemical performances of Silicon doped high-voltage cathode material. Si doping is usefull not only to stabilize the Fd3m crystal structure, but also to increase the disorder on the cationic sites. Si occupies the tetrahedral site and the corresponding amount of Li moves to the octahedral one. A solubility limit is reached for x = 0.10, and this explains the optimized electrochemical performances reported in literature for $0.05 \leq x \leq 0.15$ in $LiNi_{0.5}Mn_{1.5-x}Si_xO_4$. Silicon addition can control and limit the particle growth, in particular the formation of the octahedral morphology, typical of the spinel structures. This goal is reached not only on successfully substituted samples (BM synthesis), but also when the segregation of lithium silicate phases is observed. Lower

particle sizes can favor the lithium diffusion and improve the electrochemical performances. The rate capabilities are better for Si doped samples

AKNOWLEDGEMENTS

Fatemi sapere…io non ne ho

REFERENCES

[1] M.S. Whittingham, Ultimate limits to intercalation reactions for lithium batteries, Chem. Rev. 114 (2014) 11414-11443.

[2] M. Armand, J.M. Tarascon, Building better batteries, Nature 451 (2008) 652-657.

[3] B. Scrosati, J. Hassoun, Y.K. Sun, Lithium-ion batteries. A look into the future, Energy Environ. Sci. 4 (2011) 3287-3295.

[4] Y.-R. Zhu, T.-F. Yi, Recent progress in the electrolytes for improving the cycling stability of $LiNi_{0.5}Mn_{1.5}O_4$ high-voltage cathode, Ionics 22 (2016) 1759–1774.

[5] J. Lin, D.B. Mu, Y. Jin, B.R. Wu, Y.F. Ma, F. Wu, Li-rich layered composite $Li[Li_{0.2}Ni_{0.2}Mn_{0.6}]O_2$ synthesized by a novel approach as cathode material for lithium ion battery, J. Power Sources 230 (2013) 76–80.

[6] J. Liu, A. Huq, Z. Moorhead-Rosenberg, A. Manthiram, K. Page, Nanoscale Ni/Mn ordering in the High Voltage spinel cathode $LiNi_{0.5}Mn_{1.5}O_4$, Chem. Mater. 28 (2016) 6817−6821.

[7] H. Duncan, D. Duguay, Y. Abu-Lebdeh, I.J. Davidson, Study of the $LiMn_{1.5}Ni_{0.5}O_4$/Electrolyte interface at room temperature and 60°C, Journal of the Electrochemical Society 158 (2011) A537-A545.

[8] A. Manthiram, K. Chemelewski,E.-S. Lee, A perspective on the high-voltage $LiMn_{1.5}Ni_{0.5}O_4$ spinel cathode for lithium-ion batteries, Energy Emviron. Sci. 7 (2014) 1339-1350.

[9] J.W. Fergus, Recent developments in cathode materials for lithium ion batteries, J. Power Sources 195 (2010) 939–954.

[10] D.W. Shin, C.A. Bridges, A. Huq, M. P. Paranthaman, A. Manthiram, Role of cation ordering and surface segregation in High-Voltage spinel $LiMn_{1.5}Ni_{0.5-x}M_xO4$ (M = Cr, Fe, and Ga) cathodes for Lithium-Ion Batteries, Chem. Mater. 24 (2012) 3720−3731.

[11] Z. Moorhead-Rosenberg, A. Huq, J.B. Goodenough, A. Manthiram, Electronic and electrochemical properties of $Li_{1-x}Mn_{1.5}Ni_{0.5}O_4$ spinel cathodes as a function of Lithium content and cation ordering, Chem. Mater. 27 (2015) 6934−6945.

[12] Mukerjee, S.; Yang, X. Q.; Sun, X.; Lee, S. J.; McBreen, J.; Ein- Eli, Y. Electrochim. Acta 2004, 49, 337

[13] N.P.W. Pieczonka, Z. Liu, P. Lu, K.L. Olson, J. Moote, B.R. Powell, J.-H. Kim, Understanding Transition-Metal dissolution behavior in $LiNi_{0.5}Mn_{1.5}O_4$ High-Voltage spinel for Lithium Ion Batteries, J. Phys. Chem. C 117 (2013) 15947-15957.

[14] K.M. Shaju, P.G. Bruce, Nano-$LiNi_{0.5}Mn_{1.5}O_4$ spinel: a high power electrode for Li-ion batteries, Dalton Trans. 40 (2008) 5471-5475.

[15] T.F. Yi, X.G. Hu, Preparation and characterization of sub-micro $LiNi_{0.5-x}Mn_{1.5+x}O_4$ for 5V cathode materials synthesized by an ultrasonic-assisted co-precipitation method, J. Power Sources 167 (**2007)** 185-191.

[16] Z.-H. Xiao, Q.-Q. Cui, X.-L. Li, H.-L. Wang, Q. Zhou, Ionothermal synthesis for Mg-doped $LiMn_{1.5}Ni_{0.5}O_4$ spinel with structural stability and high-rate performance, Ionics 21 (2015) 1261–1267.

[17] J. Liu, A. Manthiram, Understanding the improved electrochemical performances of Fe-substituted 5 V spinel cathode $LiMn_{1.5}Ni_{0.5}O_4$, J. Phys. Chem. C 113 (2009) 15073–15079.

[18] T.-F. Yi, Y. Xie, M.-F. Ye, L.-J. Jiang, R.-S. Zhu, Y.-R. Zhu, Recent developments in the doping of $LiNi_{0.5}Mn_{1.5}O_4$ cathode material for 5 V lithium-ion batteries, Ionics 17 (2011) 383-389.

[19] W. Zhu, D. Liu, J. Trottier, C. Gagnon, A. Guerfi, C.M. Julien, A. Mauger, K. Zaghib, Comparative studies of the phase evolution in M-doped $Li_xMn_{1.5}Ni_{0.5}O_4$ (x = Co, Al, Cu and Mg) by in-situ X-ray diffraction, J. Power Sources 264 (2014) 290-298.

[20] K.R. Chemelewski, A. Manthiram, Origin of site disorder and oxygen non-stoichiometry in $LiMn_{1.5}Ni_{0.5-x}M_xO_4$ (M = Cu and Zn) cathodes with divalent dopant ions, J. Phys. Chem. C 117 (2013) 12465-12471.

[21] M.-L.-P. Le, P. Strobel, F. Alloin, T. Pagnier, Influence of the tetravalent cation on the high-voltage electrochemical activity of $LiNi_{0.5}M_{1.5}O_4$ spinel cathode materials, Electrochim. Acta 56 (2010) 592-599.

[22] M. Keppeler, S. Nageswaran, S.-J. Kim, M. Srinivasan, Silicon doping for High Voltage spinel $LiNi_{0.5}Mn_{1.5}O_4$ towards superior electrochemical performance of Lithium Ion Batteries, Electroch. Acta 213, (2016) 904-910.

[23] S. Nageswaras, M. Keppeler, S.-J. Kim, M. Srinivasan, Morphology controlled Si-modified $LiNi_{0.5}Mn_{1.5}O_4$ microspheres as high performance high voltage cathode materials in lithium ion batteries, J. Power Sources 346 (2017) 89-96.

[24] X. Fang, M. Ge, J. Ronga, C. Zhou, Graphene-oxide-coated $LiNi_{0.5}Mn_{1.5}O_4$ as high voltage cathode for lithium ion batteries with high energy density and long cycle life, J. Mater. Chem. A 1 (2013), 4083–4088.

[25] D. Liu, J. Hamel-Paquet, J. Trottier, F. Barray, V. Gariépy, P. Hovington, A. Guerfi, A. Mauger, C.M. Julien, J.B. Goodenough, K. Zaghib, Synthesis of pure phase disordered $LiMn_{1.45}Cr_{0.1}Ni_{0.45}O_4$ by a post-annealing method, J. Power Sources 217 (2012) 400-406.

[26] T. Yang, N. Zhang, Y. Lang, K. Sun, Enhanced rate performance of carbon-coated $LiNi_{0.5}Mn_{1.5}O_4$ cathode material for lithium ion batteries, Electochimica Acta 56 (2011) 4058-4064.

[27] H. Zhao, S. Liu , Z. Wang, Y. Cai, M. Tan, X. Liu, $LiSi_xMn_{2-x}O_4$ ($x \leq 0.10$) cathode materials with improved electrochemical properties prepared via a simple solid-state method for high-performance lithium-ion batteries, Ceram. International 42 (2016) 13442–13448.

[28] A. Iturrondobeitia, A. Goni, L. Lezama, C. Kim, M. Doeff, J. Cabana. T. Rojo, Effect of Si(IV) substitution on electrochemical, magnetic and spectroscopic performance of nanosized $LiMn_{2-x}Si_xO_4$, J. Mater. Chem. A 1(2013) 10857-10862.

[29] H. Duncan, Y. Abu-Lebdeh, I.J. Davidson, Study of the cathode-electrolyte interface of $LiMn_{1.5}Ni_{0.5}O_4$ synthesized by a sol-gel method for Li-Ion Batteries, J. Electrochem. Soc. 157 (2010) A528-A535.

[30] G.B. Zhong, Y.Y. Wang, Z.C. Zhang, C.H. Chen, Effects of Al substitution for Ni and Mn on the electrochemical properties of $LiNi_{0.5}Mn_{1.5}O_4$, Electrochimica Acta 56 (2011) 6554– 6561.